

# Generating Multipartite Spin States with Fermionic Atoms in a Driven Optical Lattice

Mikhail Mamaev<sup>1</sup> and Ana Maria Rey<sup>2</sup>

<sup>1</sup>*JILA, NIST and Department of Physics, University of Colorado, Boulder, Colorado 80309, USA*  
<sup>2</sup>*and Center for Theory of Quantum Matter, University of Colorado, Boulder, Colorado 80309, USA*

 (Received 30 January 2020; accepted 12 May 2020; published 16 June 2020)

We propose a protocol for generating generalized Greenberger-Horne-Zeilinger (GHZ) states using ultracold fermions in 3D optical lattices or optical tweezer arrays. The protocol uses the interplay between laser driving, on site interactions and external trapping confinement to enforce energetic spin- and position-dependent constraints on the atomic motion. These constraints allow us to transform a local superposition into a GHZ state through a stepwise protocol that flips one site at a time. The protocol requires no site-resolved drives or spin-dependent potentials, exhibits robustness to slow global laser phase drift, and naturally makes use of the harmonic trap that would normally cause difficulties for entanglement-generating protocols in optical lattices. We also discuss an improved protocol that can compensate for holes in the loadout at the cost of increased generation time. The state can immediately be used for quantum-enhanced metrology in 3D optical lattice clocks, opening a window to push the sensitivity of state-of-the-art sensors beyond the standard quantum limit.

DOI: [10.1103/PhysRevLett.124.240401](https://doi.org/10.1103/PhysRevLett.124.240401)

**Introduction.**—Creating useful entanglement is one of the most important goals in modern quantum research. In recent years, there has been significant effort towards generating many-body entangled states, which exhibit massive utility for quantum computation, simulation and metrology. For the latter application of metrology, an  $N$ -body fully entangled state can yield sensitivity improvement by a factor of  $\sqrt{N}$  compared to experiments using unentangled atoms or modes [1]. Such gains in precision are relevant for real-world applications such as time keeping, magnetometry and navigation, and for fundamental science including searches for dark matter and physics beyond the standard model [2].

While there has been progress on many-body entanglement generation in many fields, one of the most promising platforms is ultracold atoms. A variety of entangled states have been proposed and/or experimentally realized with such systems, including spin-squeezed states [3],  $W$  states [4], and in particular generalized GHZ states using trapped ions [5–8] or Rydberg atoms in optical tweezers [9]. However, the difficulty of combining single-site resolution with scalability has limited the fidelity and size of the states thus far, especially in systems where they can be directly used for metrological purposes.

In this work, we propose a method for generating  $N$ -particle GHZ states (also called spin cat states) using ultracold fermionic atoms loaded into a 3D optical lattice. Our protocol uses on site repulsive interactions, spin-orbit coupled (SOC) laser driving [10–12], and the harmonic trapping potential naturally generated by the curvature of the lattice beams. While we focus on 3D lattices, the setup may also be realized in optical tweezer arrays with

an ac-Stark shift gradient to emulate the trap. We describe a step-by-step generation of entanglement by creating an initially local superposition, and spatially changing one of its components while leaving the other component untouched due to energetic constraints.

Despite having site-resolved atomic motion, we do not require site-resolved focused lasers, instead only needing a collective driving laser. We also require no spin-dependent lattice potentials or lattice modulation. The drive, trap, and interactions lead to energetic constraints that only allow tunneling between one lattice site pair at a time, while all other sites are effectively decoupled. Our protocol is also robust to slow global phase drifts of the drive, because the system adiabatically follows the drive’s single-particle eigenstates throughout the evolution. After state generation, we describe a method to observe the enhanced phase sensitivity without needing many-body measurements such as parity, by instead implementing a reversal of the generation protocol. Finally, we give an augmentation to the protocol that compensates for holes in the loadout. These features together with scalability make our proposal promising for massive entanglement generation and sensitivity improvements in state-of-the-art sensors.

**Model.**—We consider a laser-driven 3D optical lattice populated by fermionic atoms in the lowest motional band, with two internal spin-like states  $\sigma \in \{g, e\}$ . We assume strong transverse confinement, restricting tunneling to an array of independent 1D chains each of length  $L$  and containing  $N$  atoms. Each chain operates in the Mott insulating regime with one atom per site ( $N = L$ ). Similar configurations can be generated in tweezer arrays. Figure 1 depicts the setup. The Hamiltonian is

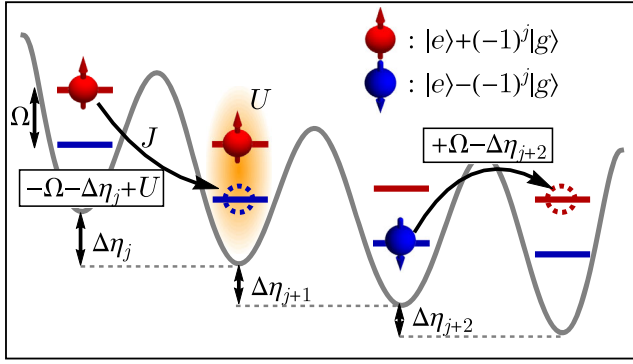


FIG. 1. Schematic of the optical lattice system, confined to 1D. The red and blue-labeled single-particle eigenstates of the collective drive field are superpositions of bare atomic states  $\{g, e\}$ , alternating due to the  $e^{ij\pi} = (-1)^j$  SOC phase in the drive. Atoms tunnel at rate  $J$  accompanied with a spin-flip due to the alternating basis. Tunneling incurs energy costs from the trap gradient ( $\pm\Delta\eta_j$ ), atomic interactions (set by  $U$ ) and driving (set by  $\Omega$ ).

$$\hat{H} = \hat{H}_{\text{Hubbard}} + \hat{H}_{\text{Drive}} + \hat{H}_{\text{Trap}}, \quad (1)$$

where  $\hat{H}_{\text{Hubbard}} = -J \sum_{\langle i,j \rangle, \sigma} (\hat{c}_{i,\sigma}^\dagger \hat{c}_{j,\sigma} + \text{H.c.}) + U \sum_j \hat{n}_{j,e} \hat{n}_{j,g}$  is the Fermi-Hubbard Hamiltonian with nearest-neighbor tunneling rate  $J$ , repulsion  $U$ , operator  $\hat{c}_{j,\sigma}$  annihilating an atom of spin  $\sigma$  on site  $j$ , and  $\hat{n}_{j,\sigma} = \hat{c}_{j,\sigma}^\dagger \hat{c}_{j,\sigma}$ . The laser  $\hat{H}_{\text{Drive}} = (\Omega/2) \sum_j (e^{ij\pi} \hat{c}_{j,e}^\dagger \hat{c}_{j,g} + \text{H.c.})$  is a collective driving field. The phase  $e^{ij\pi}$  is created by a mismatch between the driving and confining laser wavelengths, corresponding to an effective flux  $\phi = \pi$  that induces SOC [13]. We also include the trapping potential  $\hat{H}_{\text{Trap}} = \eta_{\text{ext}} \sum_j (j - j_0)^2 (\hat{n}_{j,e} + \hat{n}_{j,g})$  with trap energy  $\eta_{\text{ext}}$  from external harmonic confinement (centered on site  $j_0$ ), approximated as quadratic near the center of the lattice, yielding linear potential differences  $\Delta\eta_j = -2\eta_{\text{ext}}(j - j_0 + 1/2)$  between neighboring sites  $j$  and  $j + 1$  (See Supplementary Material [14]).

We assume that the drive frequency is much stronger than the tunneling rate,  $\Omega \gg J$ . Under this condition, the single-particle eigenstates of the system are set by the drive. We rotate into the basis of these eigenstates by defining new fermions  $\hat{a}_{j,\uparrow} = (\hat{c}_{j,e} + e^{ij\pi} \hat{c}_{j,g})/\sqrt{2}$ ,  $\hat{a}_{j,\downarrow} = (\hat{c}_{j,e} - e^{ij\pi} \hat{c}_{j,g})/\sqrt{2}$ . The Hubbard and drive Hamiltonians become

$$\begin{aligned} \hat{H}_{\text{Hubbard}} &= -J \sum_{\langle i,j \rangle} (\hat{a}_{i,\uparrow}^\dagger \hat{a}_{j,\downarrow} + \text{H.c.}) + U \sum_j \hat{n}_{j,\uparrow} \hat{n}_{j,\downarrow}, \\ \hat{H}_{\text{Drive}} &= \frac{\Omega}{2} \sum_j (\hat{n}_{j,\uparrow} - \hat{n}_{j,\downarrow}), \end{aligned} \quad (2)$$

with  $\hat{n}_{j,\tilde{\sigma}} = \hat{a}_{j,\tilde{\sigma}}^\dagger \hat{a}_{j,\tilde{\sigma}}$  for drive eigenstates  $\tilde{\sigma} \in \{\uparrow, \downarrow\}$ . The tunneling is now accompanied by a spin-flip due to the SOC phase. The trapping potential keeps the same form.

While the tunneling couples the drive eigenstates, actual transfer of atoms will depend on the energy differences between states. Some sample tunneling processes are depicted in Fig. 1. A spin- $\uparrow$  atom tunneling down the trap gradient incurs an energy change  $-\Delta\eta_j$  from the trap,  $-\Omega$  from flipping spin, and  $+U$  for creating a doublon (two atoms on one site). A spin- $\downarrow$  atom tunneling instead has a change  $+\Omega$  from the drive. If the total change is much larger than  $J$ , tunneling is suppressed. Furthermore, since the trap energy differences  $\Delta\eta_j$  vary from site to site, by making the trap strong ( $\eta_{\text{ext}} \gg J$ ) we can tune the drive frequency  $\Omega$  to resonantly enable a single tunnel coupling of a chosen spin between two chosen lattice sites while keeping all other tunneling processes off resonant. This allows for site-resolved control of lattice dynamics without needing a focused laser.

*Generation protocol.*—The control over tunneling allows us to generate a GHZ state. The scheme is depicted in Fig. 2. We assume for simplicity that the populated sites do not include the center of the trap potential ( $j_0 > L$ , with sites indexed  $j = 1, 2, \dots, L$ ). This can be achieved for example by applying a superimposed linear potential; a trap centered at the middle will be discussed afterwards. We start with a product state  $|\psi_0\rangle = \otimes_j |\downarrow\rangle_j$  [Fig. 2(a)], which can be prepared with a pulse or ramp [14]. The first step is to generate a local two-atom superposition on two adjacent sites, by resonantly enabling the tunneling of the  $\downarrow$  atom at site  $j = 1$  to  $j = 2$ . The drive frequency is set to  $\Omega = \Omega_1$ , which satisfies  $\Omega_1 + U - \Delta\eta_1 = 0$ . We keep the laser on with this frequency for a time  $tJ = \pi/4$ , realizing a unitary operation  $\hat{U}_1^{(\pi/2)} = e^{-i\hat{H}t}|_{\Omega=\Omega_1}$  equivalent to a  $\pi/2$  pulse creating an equal-weight superposition of the initial state and a doublon on  $j = 2$  [Figs. 2(b) and 2(c)]. Analogous tunneling from other sites does not occur because other trap energies  $\Delta\eta_j$  for  $j > 1$  differ by at least  $2\eta_{\text{ext}} \gg J$ .

We next force the  $j = 2$  site's  $\downarrow$  atom to tunnel to  $j = 3$ , but now, set the drive frequency to  $\Omega_2$  satisfying  $\Omega_2 - \Delta\eta_2 = 0$ . The first component of the superposition [Fig. 2(b)] will tunnel because it goes from one doublon configuration to another and suffers no penalty  $U$ . The second component [Fig. 2(c)] will have an additional cost  $U$ , its tunneling will be off resonant, and it will remain unaltered. We wait a time  $tJ = \pi/2$ , realizing a unitary  $\hat{U}_2^{(\pi)} = e^{-i\hat{H}t}|_{\Omega=\Omega_2}$  corresponding to a  $\pi$  pulse transferring the  $\downarrow$  atom from  $j = 2$  to  $j = 3$ , resulting in a new superposition [Figs. 2(d) and 2(e)]. We then make the site  $j = 3$  doublon have its  $\downarrow$  atom tunnel to  $j = 4$  with another  $\pi$  pulse (unitary  $\hat{U}_3^{(\pi)}$ ), followed by  $j = 4$  to  $j = 5$ , repeating to the end of the chain. The final state will take the form,

$$\begin{aligned} |\psi_{\text{GHZ}}\rangle &= \hat{U}_{L-2}^{(\pi)} \dots \hat{U}_2^{(\pi)} \hat{U}_1^{(\pi/2)} |\psi_0\rangle, \\ &= (|\downarrow, \downarrow, \dots, \downarrow, \downarrow\rangle + e^{i\theta_f} |0, \uparrow, \dots, \uparrow, d\rangle) / \sqrt{2}, \end{aligned} \quad (3)$$

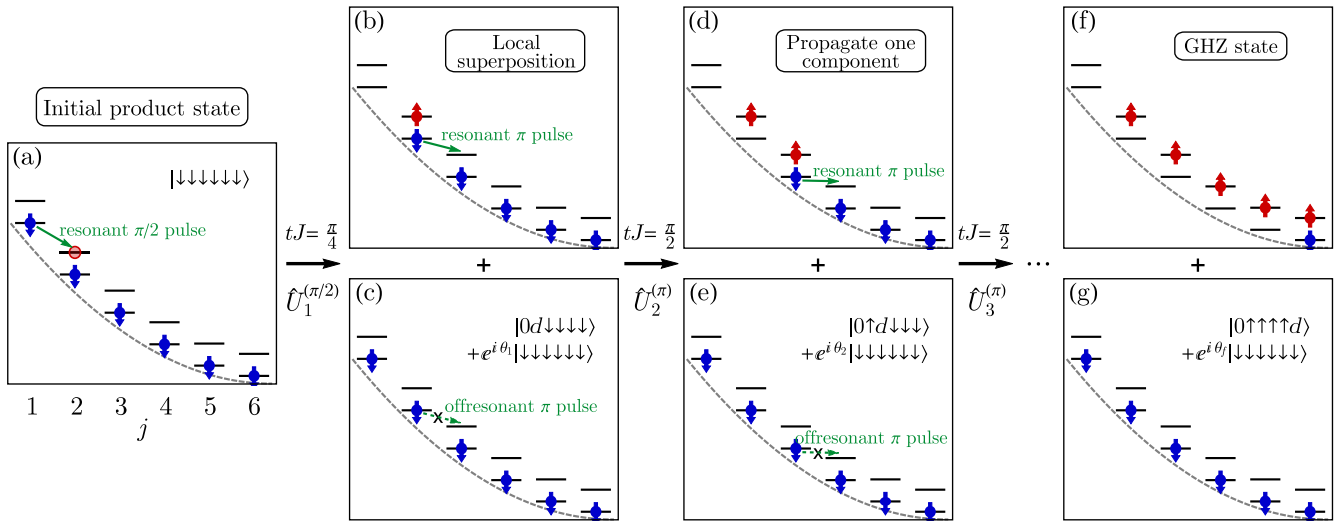


FIG. 2. Schematic of GHZ state generation protocol. The system is initialized in a product state [panel (a)]. The  $j = 1$  lattice site has tunneling enabled for its  $\downarrow$  atom, and the system is evolved for  $tJ = \pi/4$ , making an equal-weight superposition [panels (b),(c)]. The panel (b) component is allowed to tunnel further down the lattice, converting  $\downarrow$  atoms into  $\uparrow$  one site at a time with coherent transfers taking  $tJ = \pi/2$  each. The other component [panels (c),(e), corresponding to the initial state] does not evolve because of interaction-induced energy gaps. The end result is a GHZ state [panels (f),(g)]. The insets show the state at each step (with relative phases  $\theta_i$ , and  $d$  denoting doublons).

as shown in Figs. 2(f) and 2(g), corresponding to a GHZ state involving  $L$  sites,  $L - 2$  of which differ in spin projection (still assuming unit filling  $N = L$ ). Here,  $\theta_f$  is a relative phase picked up during the evolution [14], and  $d$  denotes a doublon. The total evolution time is  $tJ = \pi/4 + (L - 2)\pi/2$ . While the protocol thus far assumed that the chain did not contain the center of the trap, we can also extend it to a symmetric version ( $j_0 = L/2$ ). In this case, the superposition will have four components instead of two because each side propagates independently. Such an outcome may be useful in its own right, e.g., to create compass-type states. However, we can also prevent it from happening by disrupting the  $\hat{U}_1^{(\pi/2)}$  step on one side. Following steps will then fail on that side, allowing the protocol to proceed as before [14].

An important advantage lies in the protocol's piecewise nature. Some methods such as adiabatic dragging suffer from reduced fidelity for larger states due to exponentially shrinking many-body energy gaps with system size. Here, the reduction of the system to an effective two-level configuration at every step allows for easier optimization of the individual steps, and is conceptually straightforward to scale up. Furthermore, the evolving state exhibits some robustness to collective phase-drift effects, e.g., unwanted phases  $e^{i\lambda(t)}$  in  $\hat{H}_{\text{Drive}}$  for some function  $\lambda(t)$ . The system will follow the drift by adiabatically remaining in the drive's eigenbasis [provided  $\Omega \gg J$  and  $\lambda(t)$  varies slowly on the timescale of  $\Omega$ ], preserving the superposition. The main source of error would be imperfect resonance matching  $\delta\Omega$  between the desired and actual Rabi frequency  $\Omega_i$  at each step. Figure 3 shows a benchmark of the protocol

fidelity, averaged over trajectories with random disorder  $\delta\Omega$ . We see that GHZ states of 10 sites can be made with fidelities above 90%. Assuming a quadratic decay, we can extrapolate these results to larger states of  $L = 20$ , finding expected fidelities of  $F \approx 83\%$  with  $\delta\Omega/J = 0.25$  and  $F \approx 56\%$  with  $\delta\Omega/J = 0.5$ . This tolerance can be further improved with a deeper trap, for which the allowed  $J$  (and thus mismatch  $\delta\Omega$ ) can be larger.

*Experimental implementation and measurement.*—A feasible platform for our protocol is a 3D optical lattice [15] or tweezer array [16] loaded with quantum-degenerate fermionic alkaline earth or earth-like atoms such as Sr or Yb. The bare atomic states  $\{g, e\}$  can be represented by

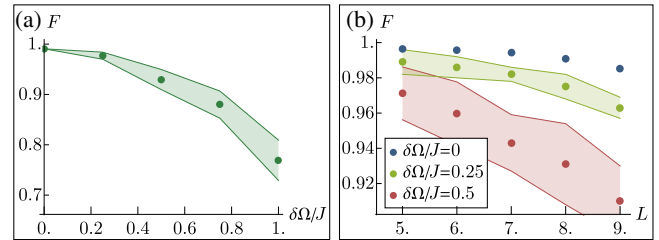


FIG. 3. (a) Fidelity of the GHZ state with drive frequency noise  $\delta\Omega$ . The deviation is implemented as a random constant shift  $\Omega_i \rightarrow \Omega_i + \delta\Omega_i$  to each step of the protocol, uniformly drawn from  $\delta\Omega_i \in [-\delta\Omega, \delta\Omega]$  (thus different for every step). Each step is simulated using exact numerical evolution under the full Hamiltonian. Multiple trajectories of randomly drawn sets  $\{\delta\Omega_i\}$  are run, and their fidelity averaged. The shaded region shows one standard deviation. Parameters are  $L = 8$  at unit filling,  $U/J = 405$ ,  $\eta_{\text{ext}}/J = 21$ . (b) Averaged fidelity as a function of  $L$ , for fixed levels of drive noise.

electronic clock states with optical frequency separation. For a lattice, the confinement should be made strong along transverse directions ( $\hat{x}$ ,  $\hat{y}$ ) and intermediate along the generation direction ( $\hat{z}$ ). A lattice using spin-polarized fermionic  $^{87}\text{Sr}$  at the magic wavelength can realize parameters of  $U/J \approx 400$ ,  $\eta_{\text{ext}}/J \approx 20$ ,  $J/(2\pi) \approx 10$  Hz [14]; deeper traps can also be made by reducing beam waist. Note that a deep enough trap can reduce  $J$  for sites far from the trap center due to wave function deformation, but this reduction should be negligible provided the nearest-neighbor energy differences  $\Delta\eta_j$  are much smaller than the band gap. Even if there is a small change to  $J$ , we only need to run those particular steps for a longer time interval. Typical generation time for these parameters is  $t \sim L \times 25$  ms, which is small compared to coherence times  $\sim 10$  s [17] for state size  $L \sim 10$  sites. The 3D lattice allows simultaneous creation of many states from which a constructive measurement signal can be obtained as described below.

To use the GHZ state for enhanced sensing, we allow it to pick up a relative phase from laser detuning, which is an additional Hamiltonian term  $(\delta/2) \sum_j (\hat{n}_{j,e} - \hat{n}_{j,g})$ . The scheme is depicted in Fig. 4(a). After generation, a pulse  $\hat{P}$  rotates the state into a form where its superposition components will acquire a relative phase  $\theta_\delta = \delta(N-1)t_\delta$  if they precess for time  $t_\delta$  ( $N-1$  because of the edge sites, [14]). Conventionally, this  $N$ -proportional enhancement is observed using a Ramsey sequence followed by a parity measurement [18–20], requiring measurement of  $N$ -body correlators which can be challenging for clocks, although it can be done in tweezers [16].

As an alternative approach, we instead undo the generation sequence, as shown in Fig. 4(a). After precession, we rotate the state back into the gauged frame with another pulse  $\hat{P}^\dagger$  [14]. We then do the  $\pi$ -pulse steps in reverse order,  $\hat{U}_2^{(\pi)}, \dots, \hat{U}_{L-2}^{(\pi)} |\psi_{\text{GHZ},\delta}\rangle$  (with  $|\psi_{\text{GHZ},\delta}\rangle$  the state after precession and applying  $\hat{P}^\dagger$ ). These steps reduce the state to  $(|\downarrow, \downarrow\rangle + e^{i(\theta_r + \theta_\delta)} |0, d\rangle) / \sqrt{2} \otimes |\downarrow, \dots, \downarrow\rangle$ , where the superposition is back on two sites  $j = 1, 2$  and  $\theta_r$  is a constant phase depending on system size and parameters. Reapplying unitary  $\hat{U}_1^{(\pi/2)}$  will rotate this state into a form where the relative phase may be measured from doublon number  $\langle \hat{n}_d \rangle = \sum_j \langle \hat{n}_{j,\uparrow} \hat{n}_{j,\downarrow} \rangle$  in the vicinity of  $j = 1, 2$ , without needing  $N$ -body correlators. The doublon number will oscillate as a function of  $t_\delta$ , allowing the detuning to be obtained from the period.

We have assumed unit filling. While unwanted holes in a 3D lattice will be confined by the energy gaps, they will interrupt state generation, leading to GHZ states of different sizes. However, sufficiently high filling will allow the maximum-length ones to dominate the signal. We benchmark the measurement protocol in Figs. 4(b)–4(e) by randomly sprinkling holes into a 3D lattice, and computing how many states of each length we get. Figure 4(b) shows

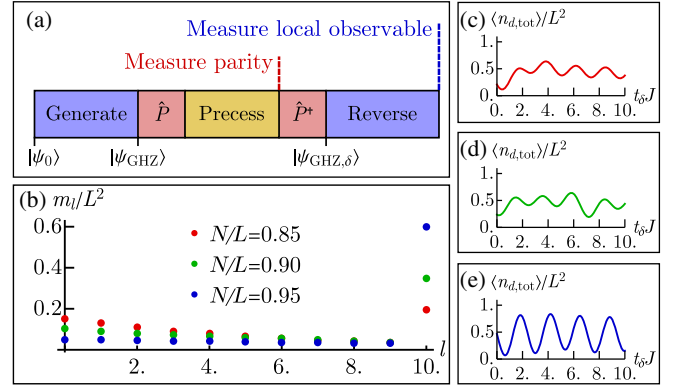


FIG. 4. (a) Schematic for using the GHZ state in metrology. A parity measurement can be done after allowing the state to precess under detuning  $\delta$  (pulse  $\hat{P}$  puts the state into the appropriate lab frame [14]). If we reverse the generation after precession, we can instead measure a local observable (doublon number). (b) Average histogram of state lengths that can be generated in a 3D lattice for randomly sprinkled holes given filling fraction  $N/L$ . See main text for definition of  $m_l$ . The lattice size is  $L \times L \times L$  with  $L = 10$ . (c)–(e) Sample trajectories of total doublon number ( $\hat{n}_d$  summed over all states according to the randomly sprinkled distribution, [14]) after reversal for different filling fractions  $N/L = 0.85, 0.90, 0.95$ , respectively. Detuning is set to  $\delta/J = 0.3$ . The bare phases  $\theta_r$  are chosen randomly from  $[0, 2\pi]$  for simplicity, but made equal for all states of a given length  $l$ .

the distribution  $m_l$  of total number of GHZ states with size  $l \in [0, 1, \dots, L]$  that can be made by starting from one edge of the lattice, counting along a given direction and stopping if we meet a hole. Figs. 4(c)–4(e) give sample oscillation trajectories of total doublon number  $\langle \hat{n}_{d,\text{tot}} \rangle$  ( $\langle \hat{n}_d \rangle$  summed over the array of states, [14]). For  $L = 10$ , fillings above  $N/L \gtrsim 0.9$  yield a clear oscillatory signal  $(10-1)$  times faster than a single unentangled atom, leading to  $\sqrt{10-1}$  times faster clock protocols [21]. One may also employ Fourier analysis to discern the contributions of different sizes.

*Hole correction protocol.*—Our protocol can be modified to compensate for small numbers of holes at the cost of longer generation time. We can augment every step of the original protocol except the first with two auxiliary steps. We first attempt to move a  $\downarrow$  atom to make a doublon on the next lattice site as normal ( $|d, \downarrow\rangle \rightarrow |\uparrow, d\rangle$ ). If an atom is missing,  $|d, 0\rangle$ , this step will fail. We then apply an auxiliary step that repeats the same tunneling process, but now assuming the target site to have no atom, allowing the transfer  $|d, 0\rangle \rightarrow |\uparrow, \uparrow\rangle$ . A second auxiliary step moves the remaining atom over,  $|\uparrow, \uparrow\rangle \rightarrow |0, d\rangle$ , and the protocol may continue. If no holes were present, neither auxiliary step would have an effect because they would be off resonant [14]. Note that the all-spin- $\downarrow$  superposition component will also suffer local changes, but these will not

propagate further, maintaining a significant difference in spin projection [14]. While this augmentation is not as useful to 3D lattice setups whose measurement signal comes from the largest-size state, it can be useful for tweezer systems.

*Conclusions.*—We have proposed a method for generating GHZ states with ultracold fermions that can be directly implemented with 3D lattice systems or tweezer arrays. The resulting state can be immediately used *in situ* for metrological purposes through a Ramsey-like sequence combined with protocol reversal. The fidelity requires good control over drive frequency, but this requirement can be made less stringent with a stronger trap, which also allows for larger tunneling rates and faster generation time. With a 2D tweezer array, one could even generate a GHZ state along one 1D tube, then repeat the protocol along a transverse axis, leading to a 2D GHZ state. One may also use a purification scheme to convert many bad GHZ states into a smaller number of good ones [22]. Altogether, this scheme offers a promising way to generate and use strongly entangled states in metrologically relevant systems.

M. M. acknowledges a CTQM graduate fellowship. This work is supported by the AFOSR Grant No. FA9550-19-1-0275, by the DARPA and the ARO Grant No. W911NF-16-1-0576, the NSF Grants No. PHY1820885 and No. NSF JILA-PFC PHY-1734006, and by NIST.

\*mikhail.mamaev@colorado.edu

- [1] C. L. Degen, F. Reinhard, and P. Cappellaro, Quantum sensing, *Rev. Mod. Phys.* **89**, 035002 (2017).
- [2] D. DeMille, J. M. Doyle, and A. O. Sushkov, Probing the frontiers of particle physics with tabletop-scale experiments, *Science* **357**, 990 (2017).
- [3] J. Ma, X. Wang, C.-P. Sun, and F. Nori, Quantum spin squeezing, *Phys. Rep.* **509**, 89 (2011).
- [4] F. Haas, J. Volz, R. Gehr, J. Reichel, and J. Estève, Entangled states of more than 40 atoms in an optical fiber cavity, *Science* **344**, 180 (2014).
- [5] C. A. Sackett, D. Kielpinski, B. E. King, C. Langer, V. Meyer, C. J. Myatt, M. Rowe, Q. A. Turchette, W. M. Itano, D. J. Wineland, and C. Monroe, Experimental entanglement of four particles, *Nature (London)* **404**, 256 (2000).
- [6] T. Monz, P. Schindler, J. T. Barreiro, M. Chwalla, D. Nigg, W. A. Coish, M. Harlander, W. Hänsel, M. Hennrich, and R. Blatt, 14-Qubit Entanglement: Creation and Coherence, *Phys. Rev. Lett.* **106**, 130506 (2011).
- [7] D. Leibfried, E. Knill, S. Seidelin, J. Britton, R. B. Blakestad, J. Chiaverini, D. B. Hume, W. M. Itano, J. D. Jost, C. Langer *et al.*, Creation of a six-atom Schrödinger cat state, *Nature (London)* **438**, 639 (2005).
- [8] N. Friis, O. Marty, C. Maier, C. Hempel, M. Holzäpfel, P. Jurcevic, M. B. Plenio, M. Huber, C. Roos, R. Blatt, and B. Lanyon, Observation of Entangled States of a Fully Controlled 20-Qubit System, *Phys. Rev. X* **8**, 021012 (2018).
- [9] A. Omran, H. Levine, A. Keesling, G. Semeghini, T. T. Wang, S. Ebadi, H. Bernien, A. S. Zibrov, H. Pichler, S. Choi, J. Cui, M. Rossignolo, P. Rembold, S. Montangero, T. Calarco, M. Endres, M. Greiner, V. Vuletić, and M. D. Lukin, Generation and manipulation of Schrödinger cat states in Rydberg atom arrays, *Science* **365**, 570 (2019).
- [10] S. Kolkowitz, S. L. Bromley, T. Bothwell, M. L. Wall, G. E. Marti, A. P. Koller, X. Zhang, A. M. Rey, and J. Ye, Spin-orbit-coupled fermions in an optical lattice clock, *Nature (London)* **542**, 66 (2017).
- [11] L. F. Livi, G. Cappellini, M. Diem, L. Franchi, C. Clivati, M. Frittelli, F. Levi, D. Calonico, J. Catani, M. Inguscio *et al.*, Synthetic Dimensions and Spin-Orbit Coupling with an Optical Clock Transition, *Phys. Rev. Lett.* **117**, 220401 (2016).
- [12] S. L. Bromley, S. Kolkowitz, T. Bothwell, D. Kedar, A. Safavi-Naini, M. L. Wall, C. Salomon, A. M. Rey, and J. Ye, Dynamics of interacting fermions under spin-orbit coupling in an optical lattice clock, *Nat. Phys.* **14**, 399 (2018).
- [13] M. L. Wall, A. P. Koller, S. Li, X. Zhang, N. R. Cooper, J. Ye, and A. Maria Rey, Synthetic spin-orbit coupling in an optical lattice clock, *Phys. Rev. Lett.* **116**, 035301 (2016).
- [14] See the Supplemental Material at <http://link.aps.org/supplemental/10.1103/PhysRevLett.124.240401> for details on state preparation, rotation and measurement, sample experimental conditions, and mitigation of holes.
- [15] S. L. Campbell, R. B. Hutson, G. E. Marti, A. Goban, N. D. Oppong, R. L. McNally, L. Sonderhouse, J. M. Robinson, W. Zhang, B. J. Bloom *et al.*, A fermi-degenerate three-dimensional optical lattice clock, *Science* **358**, 90 (2017).
- [16] M. A. Norcia, A. W. Young, W. J. Eckner, E. Oelker, J. Ye, and A. M. Kaufman, Seconds-scale coherence on an optical clock transition in a tweezer array, *Science* **366**, 93 (2019).
- [17] A. Goban, R. B. Hutson, G. E. Marti, S. L. Campbell, M. A. Perlin, P. S. Julienne, J. P. D’Incao, A. M. Rey, and J. Ye, Emergence of multi-body interactions in a fermionic lattice clock, *Nature (London)* **563**, 369 (2018).
- [18] M. M. Boyd, T. Zelevinsky, A. D. Ludlow, S. M. Foreman, S. Blatt, T. Ido, and J. Ye, Optical atomic coherence at the 1-second time scale, *Science* **314**, 1430 (2006).
- [19] N. F. Ramsey, History of early atomic clocks, *Metrologia* **42**, S1 (2005).
- [20] J. Huang, X. Qin, H. Zhong, Y. Ke, and C. Lee, Quantum metrology with spin cat states under dissipation, *Sci. Rep.* **5**, 17894 (2016).
- [21] J. J. Bollinger, W. M. Itano, D. J. Wineland, and D. J. Heinzen, Optimal frequency measurements with maximally correlated states, *Phys. Rev. A* **54**, R4649 (1996).
- [22] W. Dür, H. Aschauer, and H.-J. Briegel, Multiparticle Entanglement Purification for Graph States, *Phys. Rev. Lett.* **91**, 107903 (2003).